IAC–15–D2.4.6.30928

# OPTIMISATION OF ASCENT AND DESCENT TRAJECTORIES FOR LIFTING BODY SPACE ACCESS VEHICLES

**Federico Toso***, **Annalisa Riccardi**†, **Edmondo Minisci**‡, **Christie Alisa Maddock**§
Centre for Future Air Space Transportation Technologies
University of Strathclyde, Scotland, United Kingdom

One of the forerunners for future space access vehicles is the spaceplane, a lifting body vehicle capable of powered horizontal take-off and landing. Employing strategies from multidisciplinary design optimisation, this paper outlines the approaches and models used towards developing an integrated design platform to assess the preliminary design and performance of a spaceplane. The trajectory and control is optimised, based on different mission objectives and constraints, for the ascent and descent mission segments of a conceptual single stage to orbit vehicle, to a circular low Earth orbits from different take-off and landing sites. A modular approach is employed, dividing the mission into phases based on model discontinuities, changes in the operating environment or vehicle operation, mission objectives or constraints. The problem is reformulated by direct transcription using multiple shooting into a constrained NLP problem, and solved by a combination of genetic algorithms for a global search, and SQP plus interior point methods for local refinement with hard constraints.

## I INTRODUCTION

One of the acknowledged limitations to space operations is the launch process; currently it is reliant on expendable vertical launch vehicles that can operate only a few times per year, requiring booking up to several years in advance with large insurance fees especially in the case of small-class satellites to low Earth orbits (LEO). One forerunner for the next generation of space access vehicles are spaceplanes: lifting body vehicles optimised for powered horizontal take-off and landing aiming to capitalise on a high degree, if not full, re-usability. These are loosely classified into two design types differing on the ascent path: ground launched with a single stage to orbit (SSTO) such as Reaction Engines Skylon vehicle, or air launched from a separate aircraft, with two or more stages, such as Virgin Galactic and S3 SOAR. Conversely the descent depends on the level of control: powered to runway, unpowered glide to runway, or partially to non-recoverable as in the case of multi-stage rockets.

The concept of spaceplanes has been around since 1940s, with the first published concept occurring in 1933 for hypersonic rocket aircraft Silbervogel that was to be launched from a sled propelled by rocket engines along rails. While there have been numerous studies and experimental demonstrators since then, most of the projects were eventually dropped due to funding and numerous technological barriers mainly around the propulsion system leading to expendable multi-stage systems over full re-usable integrated engines, and thermal protection, which ultimately meant an infeasible T/W ratio.

Significant process has been made recently on overcoming various technological barriers to entry for hypersonic vehicles, such as novel propulsion[1] and thermal protection systems. Capitalising on advances in computing power, work is now being done in the area of multi-disciplinary design optimisation to better model the vehicle and environment to simulate the operational performance in order to optimise the vehicle design based on multiple different objectives and constraints during the preliminary design stage.

### I.I Approach

The design of a payload delivery mission for spaceplane, or any space access vehicle in fact, lends itself naturally to decomposition into a multiphase problem. Looking at the two atmospheric trajectories, they can each be further divided in multiple segments, as example is shown in Figure 1. With each segment, the elements defining the problem can differ: disciplinary models (e.g., propulsion modes for a hybrid engine, or in a multi-stage propulsion sys-

*PhD student, federico.toso@strath.ac.uk
†Knowledge exchange research fellow, annalisa.riccardi@strath.ac.uk
‡Lecturers, edmondo.minisci@strath.ac.uk, christie.maddock@strath.ac.uk

tem), problem objectives and constraints, level of fidelity needed within the models, and so forth. To allow such a flexibility in the design the simulation needs to been structured in multiple phases, with interchangable software models. For each phase, the set of models used, and all the parameters involved in the parameterisation of the controls and propagation of the trajectory need to be defined. The switching between phases is controlled by the optimiser through constraints functions. This multiphase approach is also beneficial when dealing with discontinuities within the mathematical models, for example in the aerodynamics at Mach 1, which can cause difficulties with gradient-based optimisation approaches.

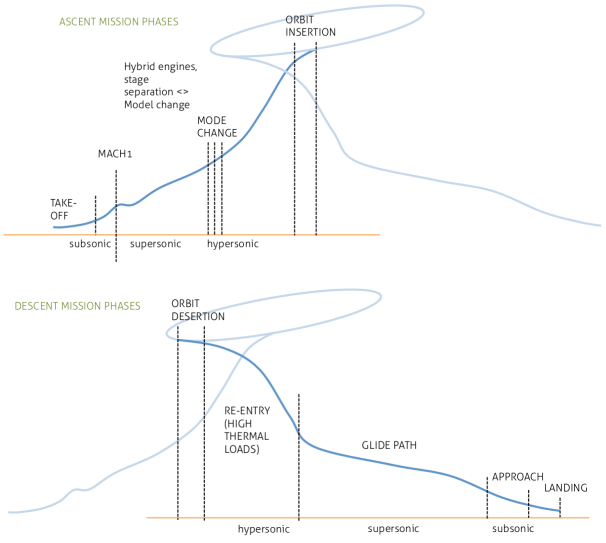


Fig. 1: Ascent and Descent trajectory phases

The simulation code used in the presented experiments has been designed to be modular. As presented in Figure 2, different disciplinary models can be included in the platform and are programmed to ensure compatibility. Different optimisation algorithms have been included and tested to tackle a variety of problem definitions – from single to multi-objective, deterministic and stochastic, from constrained to unconstrained – and to offer both global exploration capabilities, and local refinement. Fixed step size integration techniques (Runge-Kutta up to order 4 and Adams 4th-order predictor/corrector) and interpolation methods (linear interpolation, piecewise cubic Hermite interpolation) are also included. The platform is being developed in Matlab with some modules, e.g., disciplinary and atmospheric models, ported to C to improve the computational run time.

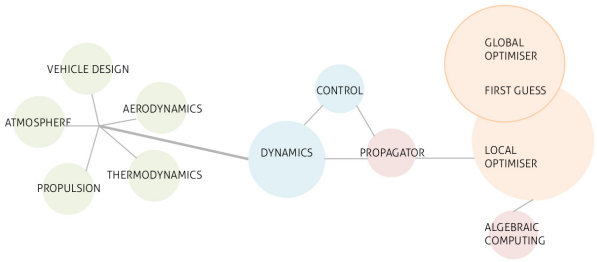


Fig. 2: Simulation environment

The following paper presents some initial results for the ascent and descent phases, which represent the more difficult problems due to the high degree on non-linearity in atmospheric flight, compared to say the control needed within the orbital phase. A test mission was used that would take-off and land at the ESA ground station in Kourou, and deposit a payload into a 300 km altitude, circular low Earth orbit (LEO). The paper first presents the methodology, describing the mathematical models used for the vehicle design and operational environment, and the optimisation algorithms employed, and concludes with some results and discussion. The objective of the powered ascent phase is to maximise the payload mass into orbit. This is equivalent to minimising the required amount of on-board propellant, assuming a fixed dry structural mass of the vehicle. Constraints were added on the dynamic loading, and the maximum normal and axial accelerations. The descent trajectory was optimised independently for to minimise the thermal loads with additional constraints on the maximum temperatures.

The vehicle design is a conceptual SSTO, nicknamed CFASTT-1, developed at the University of Strathclyde as a testing and teaching tool.[2] It is based on the Skylon vehicle design from Reaction Engines,[3] with a hybrid air-breathing and rocket propulsion system.

## II MATHEMATICAL MODELS

The following section presents the mathematical models used to simulate the vehicle performance, specifically the vehicle structure and mass, aerothermodynamics, and propulsion system, and the trajectory dynamics and control, gravitational and atmospheric models.

### II.I Vehicle design

The vehicle design is conceptual construct based on the Skylon vehicle by Reaction Engines Ltd. It is modelled through a set of engineering models that describe the behaviour of the subsystems via surrogate or low fidelity models that characterize the performance of the vehicle without excessively impacting on the computation time.

#### *II.I.1 Aerothermodynamics*

The aerodynamics of the vehicle are modelled to predict the total coefficient of lift $c_L$ and drag $c_D$ as a function of the angle of attack $\alpha$, Mach number $M$ for a set of atmospheric conditions. For the test case presented here, the aerodynamics and propulsion models were both designed as surrogate models, with curve fitting based on higher fidelity simulations using CFD for the continuum regime (lower atmosphere) and Direct Simulation Monte Carlo (DSMC) based methods for the upper atmosphere assuming a rarefied flow regime.[4] The surrogate models were necessary to lower the computation run time, compared to the higher fidelity simulations which are generally infeasible to incorporate into a complex design optimisation.

In the subsonic and supersonic regimes, the coefficient of lift is modelled based on linearised aerodynamic theory,[5]

$$C_{L,ss} = C_{L_\alpha} \sin\alpha \cos\alpha \qquad [1]$$

where $C_{L_\alpha}$ was a piecewise fitted cubic polynomial based on Mach number. The coefficient of lift within the hypersonic regime is modelled based on modified Newtonian theory,

$$C_{L,hs} = 2\sin^2\alpha \frac{S_{hyp}}{S_{ref}} \cos\alpha \qquad [2]$$

The two values of $C_L$ for the different regimes are weighted with the following equation that smooths the transition between the two:

$$C_L = \frac{C_{L,ss} + C_{L,hs}}{2} + \sqrt{C_{L,ss}^2 + C_{L,hs}^2} \qquad [3]$$

The drag coefficient is calculated as the sum of a $C_{D_0}$ term and the induced drag of lifting surfaces. The zero-lift drag term accounts for wave, base and viscous drag and is function of the Mach number. Similarly to the $C_{L_\alpha}$ term, $C_{D_0}$ was approximated by a $10^{\text{th}}$ order polynomial derived through curve fitting to higher fidelity simulations.

$$C_D = C_{D_0}(M) + C_L \tan\alpha \qquad [4]$$

The lift and drag forces used within the dynamic model are given by,

$$L = \frac{c_L \rho v^2 S_{ref}}{2} \qquad [5]$$

where $\rho$ is the atmospheric density, $v$ is the relative velocity and $A_{ref}$ is the reference area.

The thermodynamic model, used primarily in the upper phase of the re-entry, evaluates the heat flux and wall temperatures along key areas. The convective heat flux $\dot{q}_{conv}$ was modelled using the Fay-Riddell equation corrected for the hot wall temperature $T_W$ is:[6]

$$\dot{q}_{conv} = K\sqrt{\frac{\rho}{R_C}} v^3 \left(1 - \frac{H_W(T_W)}{H_{ST}}\right) \qquad [6]$$

where $R_C$ is the local radius of curvature of the geometry, $\rho$ is the atmospheric density, $v$ the flight velocity, $K$ is an empirical constant, $H_W$ is the enthalpy on the wall and $H_{ST}$is the static enthalpy of the incoming flow.

The radiative head flux is derived using the StefanBoltzmann law:

$$\dot{q}_{rad} = \epsilon\sigma(T_W^4 - T_h^4) \qquad [7]$$

where $\sigma$ is the StefanBoltzmann constant and $\epsilon$ is the emissivity of the body.

Setting $\dot{q}_{conv} = \dot{q}_{rad}$, these two equations are solved numerically to obtain the wall temperature on the nosecap $T_W$.

The wing leading edge and the nacelle are considered cylindrically inclined shapes and require a correcting function based on the sweep angle of the surface $f(\theta_{sw})$.

$$\dot{q}_{conv} = K\sqrt{\frac{\rho}{R_C}} v^3 \left(1 - \frac{H_W}{H_{ST}}\right) f(\theta_{sw}) \qquad [8]$$

Where $\theta_{sw}$ is the inclination angle of the geometry with respect to the incoming flow and is equal to the leading sweep angle for the wing and the angle of attack for the nacelle. The constants $K$, $C$ are empirically determined through CFD analyses on the vehicle.

#### *II.I.2 Propulsion*

This preliminary design study has been conducted assuming a hybrid air-breathing/rocket propulsion system similar to SABRE under development by Reaction Engines Ltd. The air-breathing propulsion system is modelled on a turbojet-ramjet configuration which has been evaluated at set points and then

curve fitted to extrapolate a faster surrogate model for preliminary design purposes. This model gives a maximum $I_{sp}$ of about 3000 s.

The upper phase of the ascent trajectory is powered by two cryogenically cooled LOX/LH2 rocket engines each with an $I_{sp}$ of 450 s. The thrust and mass fuel flow rate are calculated using the general rocket equation,

$$T_{max} = (\dot{m}_h + \dot{m}_o)\, g_0\, I_{sp} - p\, A_e = \dot{m}_p\, g_0\, I_{SP} - p\, A_e \quad [9]$$

For the purpose of this study, the mixture ratio is assumed constant and the two propellants are treated as a single mass flow. A penalty proportional to atmospheric pressure $p$ and nozzle exit area $A_e$ is introduced to account for the effect of incorrect nozzle expansion when not in a vacuum.

A throttle control $\tau$ is added, which dictates the fraction of maximum thrust applied, as well as the fraction of total propellant mass flow. The maximum thrust available is $T_{max}$=400 kN for each of the 2 rocket engines, and the mass flow is calculated with the inverse of the general rocket equation 9.

$$T = \tau T_{max} \qquad \dot{m}_p = \frac{T}{g_0 I_{SP}} \quad [10]$$

## II.II Operating environment

The Earth is modelled as a perfect sphere with a radius $R_{\text{E}} = 6375253$ m and angular velocity $\omega_{\text{E}} = 7.292115 \times 10^{-5}$ rad/s. The Earth's gravitational acceleration is a function of altitude $h$ above the surface,

$$g = \mu_{\text{E}}/r^2 = \mu_{\text{E}}/(h + R_{\text{E}})^2 \quad [11]$$

where $\mu_{\text{E}} = 398600.4418$ km$^3$/s$^2$.

Two basic globally-averaged atmospheric models were used:[7] the US Standard Atmosphere 1962 and International Standard Atmosphere (ISA). Given the altitude $h$ the models compute the value of atmospheric pressure $P$ and temperature $T$, which were then used to determine the air density $\rho$ and speed of sound $a$. The models divide the atmosphere into layers with linear temperature distributions against geopotential altitude. The values of pressure and density are computed by simultaneously solving the vertical pressure variation and the ideal gas law equations. The two models differ for altitude values above 50 km where they have divergent values for the temperature.

## II.III Trajectory dynamics

The dynamics for the transatmospheric flight are the same for ascent or descent. Within this model, the spaceplane is considered as a point with a time-varying mass centred on the Centre-of-Mass of the vehicle. The set of equations of motion are calculated within a geocentric rotating reference frame using spherical coordinates, denoted by $\mathcal{F}$.

The state vector for the position and velocity is $\mathbf{x} = [h,\, \lambda,\, \theta,\, v,\, \gamma,\, \chi]$ where $h$ is the altitude (the radial distance is $r = h + R_{\text{E}}$), $(\lambda, \theta)$ are the geodetic latitude and longitude, $v$ is the magnitude of the relative velocity vector directed by the flight path angle $\gamma$ and the flight heading angle $\chi$. The equations of motion are given by,[8]

$$\dot{h} = \dot{r} = v \sin\gamma \quad [12a]$$

$$\dot{\lambda} = \frac{v \cos\gamma \sin\chi}{r} \quad [12b]$$

$$\dot{\theta} = \frac{v \cos\gamma \cos\chi}{r \cos\lambda} \quad [12c]$$

$$\dot{v} = \frac{F_T \cos(\alpha + \epsilon) - D}{m} - g \sin\gamma + \omega_e^2 r \cos\lambda\, (\sin\gamma \cos\lambda - \cos\gamma \sin\chi \sin\lambda) \quad [12d]$$

$$\dot{\gamma} = \frac{F_T \sin(\alpha + \epsilon) + L}{mv} \cos\mu - \left(\frac{g}{v} - \frac{v}{r}\right) \cos\gamma + 2\omega_{\text{E}} \cos\chi \cos\lambda + \omega_{\text{E}}^2 \left(\frac{r}{v}\right) \cos\lambda\, (\sin\chi \sin\gamma \sin\lambda + \cos\gamma \cos\lambda) \quad [12e]$$

$$\dot{\chi} = \frac{L}{mv \cos\gamma} \sin\mu - \left(\frac{v}{r}\right) \cos\gamma \cos\chi \tan\lambda + 2\omega_{\text{E}} (\sin\chi \cos\lambda \tan\gamma - \sin\lambda) - \omega_{\text{E}}^2 \left(\frac{r}{v \cos\gamma}\right) \cos\lambda \sin\gamma \cos\chi \quad [12f]$$

where $\alpha$ is the angle of attack, $\mu$ is the bank angle, $m$ is the mass of the vehicle, $F_T$ is the magnitude of the thrust given by the engine, $\epsilon$ is the pitch offset angle between the direction of thrust $F_T$ and the longitudinal plane of the vehicle, $g$ is the gravitational acceleration, and $L$ and $D$ are the aerodynamic lift and drag forces, respectively. With the exception of $\epsilon$, all the terms are time-varying.

Looking at a standard aircraft body-relative reference frame $\mathcal{B}$, $+x^{\mathcal{B}}$ is towards the nose along the longitudinal axis of the spaceplane, $+y^{\mathcal{B}}$ is outwards along the wing, and $+z^{\mathcal{B}}$ points downwards towards the Earth normal to the plane of symmetry given by $x^{\mathcal{B}}$-$y^{\mathcal{B}}$. The flight path angle is the angle between the local horizon (defined by as the plane tangent to the radial vector) and the velocity vector, while the flight heading angle is the angle between North (or the $x^{\mathcal{F}}$-axis) and the horizontal component of the velocity vector.

For the orbital dynamics, a standard two-body

system was used, based on a closed orbit around a central body with a gravitational field. An elliptical transfer trajectory is found by numerically solving Lambert's problem using Battin's method,[9,10] which aims to solve the boundary value problem for,

$$\ddot{r} = -\mu_{\mathrm{E}} \frac{\hat{r}}{r^2} \qquad [13]$$

given a starting and ending position vector, in Earth Centred Inertial (ECI) coordinates, and a total time-of-flight.

The state vector $\mathbf{x}^{\mathcal{F}}$ was transformed into the ECI reference frame via the Earth Centered Earth Fixed (ECEF) frame using the conversions defined by the IAU Resolutions.[11]

## III OPTIMISATION

### III.I Optimal control problem

The problem of optimizing the ascent and descent trajectory is an optimal control problem. Optimal control seeks the control laws for a given system that minimizes a cost functional subject to initial and final states as well as path constraints. This is an infinite dimensional optimization problem, for which usually it is not possible to find the exact analytic solution, hence the need of a numerical method for approximating its solution. Numerical methods are divided into indirect and direct methods.

Direct methods are the most robust methodology to solve optimal control problems. The main idea of the techniques is to discretise the control and state functions, and transform the infinite dimensional optimal control problem into a finite dimensional Non Linear Programming (NLP) problem. The disadvantage of this approach is that the objective function and the constraints on the optimization can only be evaluated at the end of the simulation. Transcription by the single shooting approach results in a NLP problem with a relatively small number of independent design variables, but dynamical systems which are subject to instability for certain values of their control parameters (as is often the case) are difficult to treat with this method.

A multiple shooting method instead divides the time in multiple shooting segments $[t_0, t_1, ..., t_M]$, where the trajectory is integrated numerically within the interval $[t_i, t_{i+1}]$ with initial conditions $x_i$, for all $i = 0, ..., M-1$. The state vector is given by,

$$\dot{x}(t) = f(x(t), u(t)), \quad x(t_i) = x_i \;\; t \in [t_i, t_{i+1}] \qquad [14]$$

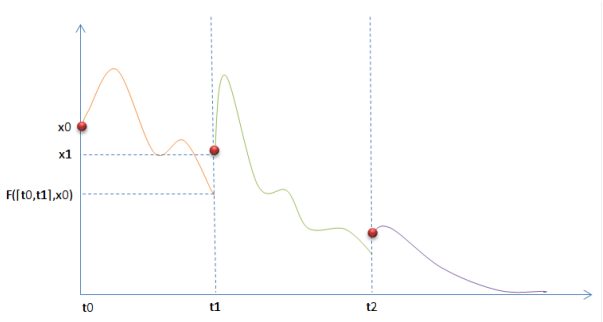


Fig. 3: Multiple shooting discretisation

With each interval $[t_i, t_{i+1}]$, the control is further discretised in $NC$ control nodes: $\{u_0^i, ..., u_{NC}^i\}$ for $i = 0, ..., M-1$ (see Figure 3). Continuity constraints on the control and states need to be imposed for $i = 1, ..., M-1$,

$$x_i = F([t_{i-1}, t_i], x_{i-1}), \quad u_{NC}^{i-1} = u_0^i \qquad [15]$$

where $F([t_{i-1}, t_i], x_{i-1})$ is the final state of the numerical integration on the interval $[t_{i-1}, t_i]$ with initial conditions $x_{i-1}$. This has the benefit of reducing integration errors often present over long integration times, and more importantly, can deal with discontinuities by aligning the transition between phases with any mathematical discontinuities within the models. The trade-off is the steep increase in the number of optimisation variables.

The optimization problem therefore has the following control variables:

- The state vector at the state of each shooting phase $\mathbf{x}_i$, for $i = 0, ..., M-1$
- The control nodes $\{\mathbf{u}_0^i, ..., \mathbf{u}_{NC}^i\}$, for $i = 0, ..., M-1$,
- The time of flight for each shooting phase $t_i$, for $i = 1, ..., M$

For the given problem, path constraints on maximum temperatures, axial and normal accelerations have also been included in the optimization problem formulation. Additional equality constraints on the final orbit, in the case of the ascent, or final landing point in the case of descent are added to the problem.

### III.II First guess

Different strategies to provide a good first guess to the optimiser were used.

For the descent, a single integration of the trajectory from a given initial state is used (i.e., single

shooting). The trajectory is integrated from given initial conditions and constant controls till the reaching of the final orbit or the landing site altitude. The final trajectory is subdivided in the $M$ segment of the multiple shooting transcription method used. The state variables $x_i$ in the multiple shooting nodes are initialized with the corresponding state value of the reference trajectory and the control are kept constant, $u_j^i = U$ for all $i = 0, ..., M-1$ and for all $j = 0, ..., NC$. The multiple shooting time length $t_i$ is initialized to zero.

Alternatively the quick run of the stochastic global search is the first guess strategy used in the case of the ascent. This is largely due to the shorter time of flight required for the ascent trajectory, requiring less multiple shooting segments. The resulting optimization problem has a smaller number of equality constraints so it can be more easily solved with a global stochastic strategy that includes the constraints in the objective function as penalty parameters. The Matlab genetic algorithm `ga` was used in the test case here.

### III.III Optimization algorithm

The NLP problem is solved using the Sequential Quadratic Programming (SQP) algorithm with `fmincon` in MATLAB subject to a number of equality and inequality constraints. The SQP algorithms employs Newton-like methods to directly solve the necessary conditions for optimality (KKT conditions) of the original NLP problem. The problem to be solved is transformed into the minimization of a quadratic approximation of the Lagrangian function subject to a linear approximation of the constraints. A sequence of quadratic problems need to be solved in order to converge to the local optimum.

## IV TEST CASE

A test mission was analysed that would take take-off and land at the ESA Kourou launch site near the equator, located at latitude $\lambda = 5.2372$ deg N and longitude $\theta = 52.7606$ deg W. The spaceplane will deliver a payload to a 300 km altitude circular equatorial orbit, with semi-major axis $a = R_{\text{E}} + 300$ km, and eccentricity $e$, inclination $i$, right ascension of the ascending node $\Omega$ and argument of perigee $\omega$ all set equal to zero. The operational orbit segment is neglected here, with the optimisation looking at only the ascent and descent trajectories.

### IV.I Ascent

The control vector for ascent trajectory problem is $\mathbf{c} = [t, \alpha, \mu, \tau]$ where $t$ is the time coordinates of each control node within a phase. As the control law is discrete and characterized by a vector of 8 equally spaced points for each shooting phase, the evaluation of each of the parameters – the angle of attack $\alpha$, bank angle $\mu$ and throttle $\tau$ – is interpolated using a piecewise cubic Hermite interpolation scheme. The search space $D$ is constrained by the following bounds: $\alpha \in [-10, 30]$ deg, $\mu \in [-30, 30]$ deg, $\tau \in [0, 1]$ with the total flight duration for each shooting phase between 30 s and 190 s. There are 5 shooting phases, with the entire trajectory is constrained between 150 s and 850 s.

The state vector is bounded such that the altitude $h \in [0, 1000]$ km, velocity $v \in [0.1, 10]$ km/s, flight path angle $\gamma \in [-180, 180]$ deg, flight heading $\chi \in [-90, 90]$ rad, latitude $\lambda \in [-90, 90]$ deg, and longitude $\theta \in [-180, 180]$ deg.

The objective of the optimisation is to maximise the payload mass that can be injected into orbit. If the structural dry mass of the vehicle at take-off is fixed, along with a known maximum wet mass including payload, then the two free variables are the total mass of on-board propellant, and the payload mass. The objective function is therefore,

$$\min_{c \in D} m(t = t_f) \qquad [16]$$

where $\dot{m} = -\dot{m}_p$.

The initial parameters for the state vector for the ascent are:

$$h(t=0) = 10 \text{ km}$$
$$v(t=0) = 0.4 \text{ km/s}$$
$$\gamma(t=0) = \chi(t=0) = 0 \text{ deg}$$

with the latitude and longitude given above.

Additional constraints are imposed on the problem by the maximum acceleration along the longitudinal axis $a_x \leq 3g_0$ m/s$^2$ and normal axis $a_z \leq 2g_0$ m/s$^2$.

#### *IV.I.1 Descent*

The descent trajectory is divided into 3 main segments: a powered de-orbit, an unpowered re-entry through the upper atmosphere, and an unpowered glide phase in the lower atmosphere.

The de-orbit phase is defined as the trajectory above an altitude of 120 km, the nominal start of the

atmosphere. While the ascent case uses the rocket engines to reach the desired orbit, for the descent, an elliptical transfer trajectory was used instead. The trajectory assumed two impulsive $\Delta v$, one to change from the orbit to the transfer trajectory, and a second to re-align the velocity vector at the start of the re-entry.

The control variables for the de-orbit are $\mathbf{c}_1 = [\theta_0,\ tof,\ \mathbf{x}(t_{0,d})]$, where $\theta_0$ is the departure true anomaly of the orbit, and $tof$ is the total time of flight of the transfer. The values of the state vector $\mathbf{x}_{re}$, specifically the velocity, flight path angle, heading angle, longitude and latitude at the transition point between the de-orbit and re-entry is also added to the control vector, with the exception of the altitude which is fixed at 120 km. The objective function for this segment is,

$$\min_{c_1 \in D} \Delta v \qquad [17]$$

The control vector is bounded as follows: $\theta \in [0,\ 2\pi]$ rad, $tof \in [0, 2T_{orbit}]$ s where $T_{orbit}$ is the period of the operation orbit. The initial guess was set at $\theta = \pi/10$ rad and $tof = 0.5T_{orbit}$.

This re-entry and glide segments requires a different search space limitation by imposing $\alpha \in [-5.0, 60]$ deg, $\mu \in [-5, 90]$ deg, and the total flight is set as the total time of flight of the initial guess, later optimised to match the constraints on the target landing site. The state vector limits are kept the same.

The first guess for the initial state of the re-entry/glide is given as:

$$\begin{aligned} lv(t = t_{0,d}) &= 7.8754 \text{ km/s} \\ \gamma(t = t_{0,d}) &= -1.18 \text{ deg} \\ \chi(t = t_{0,d}) &= 90 \text{ deg} \\ \lambda(t = t_{0,d}) &= 0 \text{ deg} \\ \theta((t = t_{0,d})) &= 0 \text{ deg} \end{aligned}$$

where $t_{0,d}$ is the initial time of the segment.

This case requires additjional constraints due to the harsh thermal environment typical of re-entry. The heat flux and heat load are evaluated using the thermal model with temperatures evaluated at three different critical points: the nosecone, the wing leading edge and the engine nacelle. The following constraints on the temperature are considered along the whole trajectory:

$$\begin{aligned} T_{\text{nosecap}} &< 2000\,K \\ T_{\text{wing}} &< 2000\,K \\ T_{\text{nacelle}} &< 1050\,K \end{aligned} \qquad [18]$$

A reduced constraint on the maximum normal acceleration is imposed such that $\mathbf{a}_z \leq 1.5 g_0$ m/s$^2$.

The objective function for the descent trajectory is the minimisation of the integral of the heat flux:

$$\min_{\mathbf{c}_2} \int_{t_{0,d}}^{t_f} \dot{q}(t, \mathbf{c}_2)\, dt \qquad [19]$$

where $\mathbf{c}_2$ is the set of optimization variables described above and $t_f$ is the optimisable time of flight.

## IV.II Simulation results

The ascent trajectory is optimized to achieve circular orbit while satisfying all the constraints. The achieved result is on a slightly inclined plane ($i < 6$ deg) due to the fact that the equatorial condition has not been imposed to increase the convergence rate of the problem.

The ascent trajectory plots are shown in Figures 4–9 and highlight the evolution of the solution from the first guess that is given to the genetic algorithm and further refined with the gradient method to the end result of the optimized trajectory. The air-breathing phase of the trajectory is plotted with a dotted line, while the rocket powered section is displayed with a continuous line.

Fig. 5 shows the effect of the acceleration limits in the constraints of the problem. When the vehicle gets lighter, the Thrust of the rocket engine is excessive and it is gradually throttled down to a safe level. Furthermore it can be noted that the optimization algorithm develops a strategy of coasting with low thrust till the apogee to minimise the required $\Delta V$ to circularize the orbit. This effect is also noticeable in Fig. 7, from t=300 s to t=600 s, where the speed of the spaceplane increases slower.

The time history of the state variables shows that the starting guess control law is not able to sustain flight and the vehicle falls below the surface of the earth, stopping the integration routine.

The descent trajectory is shown in Figures 10–16. In the thermally unconstrained case, the nacelle and the nose reach critical temperature levels as can be seen in Fig. 15, but the introduction of the constraints stop this behaviour and modify the descent path, slowing down the descent of the vehicle by increasing the angle of attack and therefore reducing the ballistic coefficient. This stops the occurrence of the atmospheric skipping that can be seen in the first 200 seconds in Fig. 10–11 and that was causing a very steep and fast descent that was the origin of excessive heating in the unconstrained case. The last

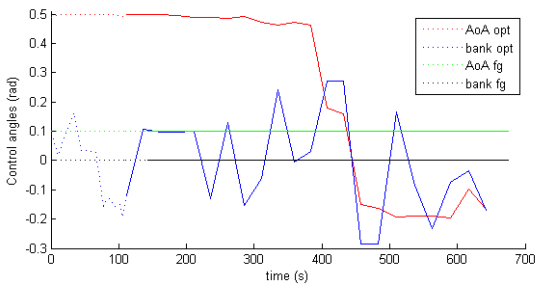


Fig. 4: Control law for angle of attack and bank angle. The green and black lines show the starting guess respectively for $\alpha$ and $\mu$, while the red and blue lines show the optimised solutions.

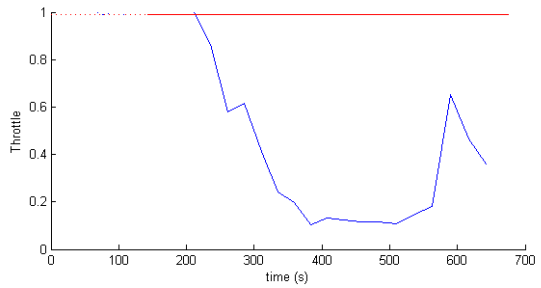


Fig. 5: Control law for Throttle, starting guess in red, optimized control law for throttle in blue, the dashed section is the air-breathing phase, the continuous is the rocket one.

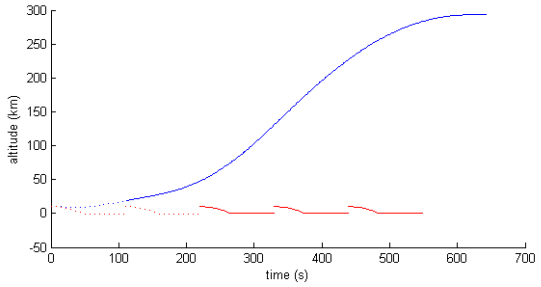


Fig. 6: Time history of the altitude during ascent, starting guess in red, optimized solution in blue, the dashed section is the air-breathing phase, the continuous is the rocket.

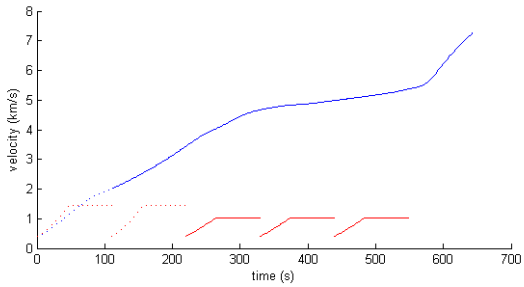


Fig. 7: Time history of the velocity, starting guess in red, optimized solution in blue, the dashed section is the air-breathing phase, the continuous is the rocket.

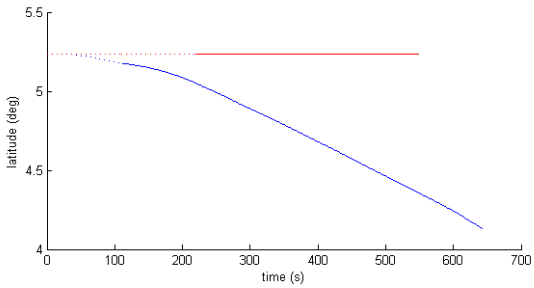


Fig. 8: Time history of the latitude, starting guess in red, optimized solution in blue, the dashed section is the air-breathing phase, the continuous is the rocket.

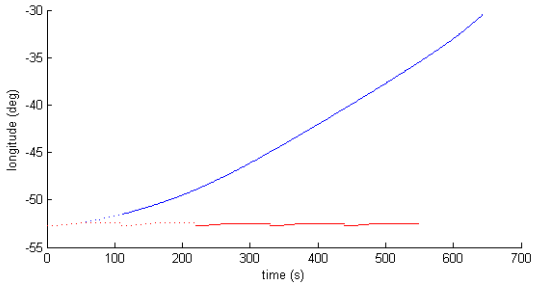


Fig. 9: Time history of the longitude, starting guess in red, optimized solution in blue, the dashed section is the air-breathing phase, the continuous is the rocket.

part of the descent is the gliding section and the obtained results are unrealistic due to the fact that the aim of this analysis was to minimize the heating during re-entry, while a more realistic objective for this particular flight phase is to maximise the lift to drag ratio and correctly align the vehicle with the landing runway.

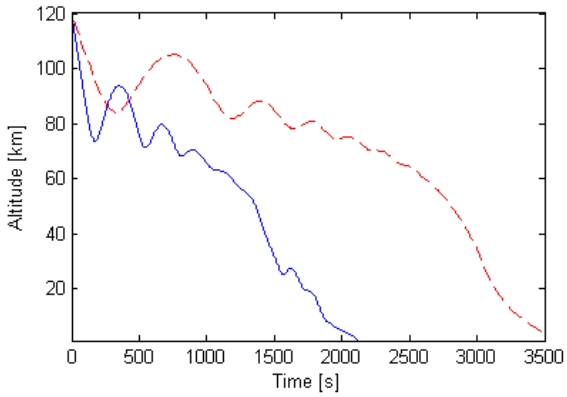


(a) With no thermal constraints

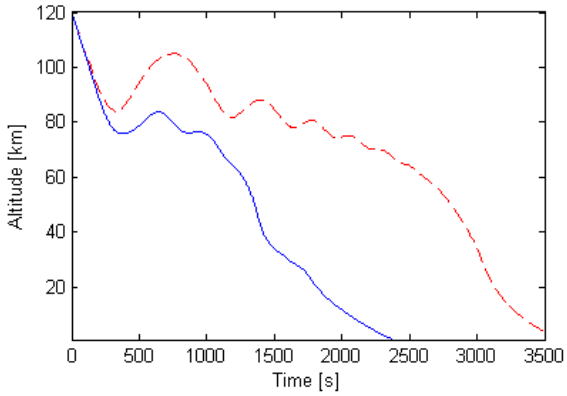


(b) With thermal constraints

Fig. 10: Time history of the altitude during the re-entry and glide phases of the descent trajectory, where the red dashed line shows the first guess, and the blue line shows the fully optimised solution.

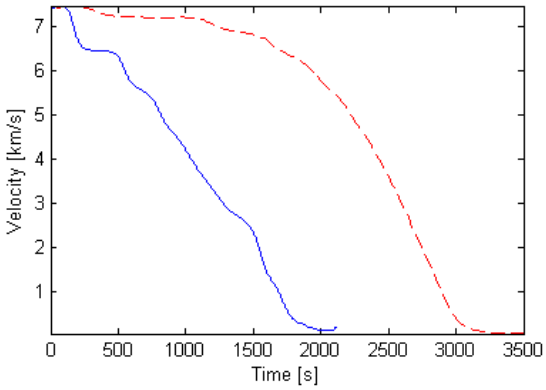


(a) With no thermal constraints

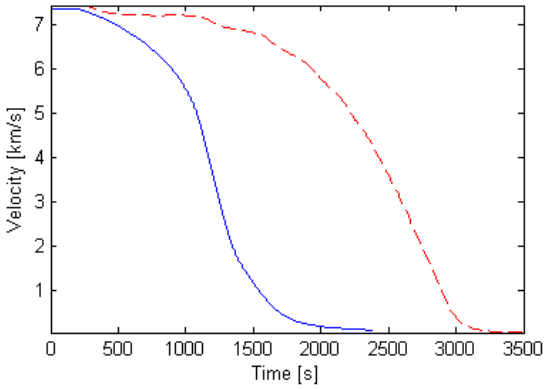


(b) With thermal constraints

Fig. 11: Time history of the velocity during the re-entry and glide phases of the descent trajectory, where the red dashed line shows the first guess, and the blue line shows the fully optimised solution.

## V CONCLUSION

This paper has outlined the approach and the models for a preliminary design and performance evaluation of a hybrid engine SSTO vehicle. It has also presented preliminary results for a full mission test case of ascent and descent trajectories to an equatorial 300 km circular orbit. The strategy of separating different flight phases that would otherwise present discontinuities is possible thanks to the modularity of the platform, leveraging the multi-shooting approach and accounting for different flight conditions. This is a further step toward the creation of an automated design platform that has modularity and flexibility at its core, allowing the solution of multiple different problems.

## ACKNOWLEDGMENTS

This research is partially supported by the UKSA NSTP-2 Pathfinder Grant RP10G0348B11.

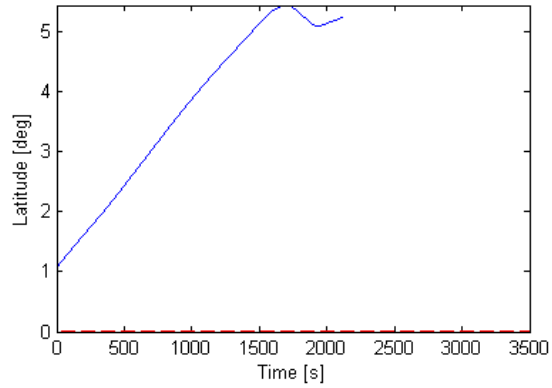


(a) With no thermal constraints

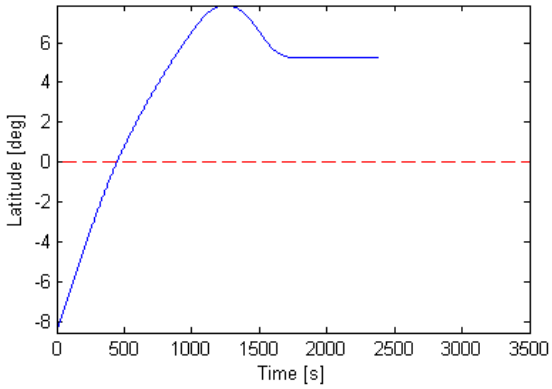


(b) With thermal constraints

Fig. 12: Time history of the latitude during the reentry and glide phases of the descent trajectory, where the red dashed line shows the first guess, and the blue line shows the fully optimised solution.

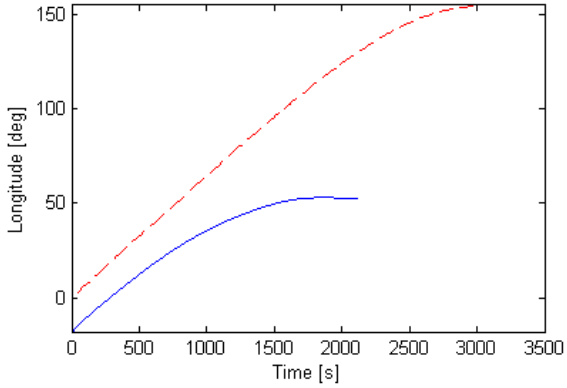


(a) With no thermal constraints

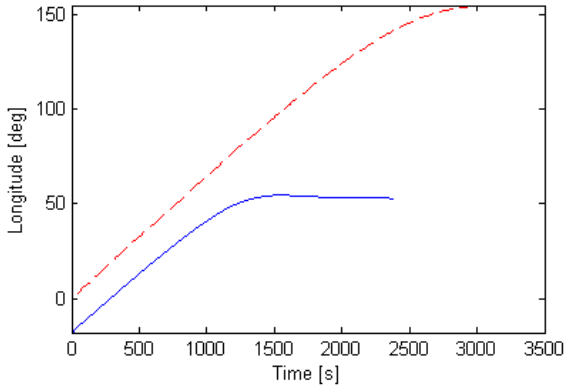


(b) With thermal constraints

Fig. 13: Time history of the longitude during the reentry and glide phases of the descent trajectory, where the red dashed line shows the first guess, and the blue line shows the fully optimised solution.

## REFERENCES

[1] Varvill, R. and Bond, A., "A comparison of propulsion concepts for SSTO reusable launchers," *JOURNAL-BRITISH INTERPLANETARY SOCIETY*, Vol. 56, No. 3/4, 2003, pp. 108–117.

[2] Wuilbercq, R., Ahmad, A., Scanlon, T., and Brown, E., "Towards Robust Aero-Thermodynamic Predictions for Re-Usable Single-Stage to Orbit Vehicles," *18th AIAA/3AF International Space Planes and Hypersonic Systems and Technologies Conference. Tours, France*, 2012.

[3] Longstaff, R. and Bond, A., "The skylon project," *AIAA Paper*, Vol. 2244, 2011, pp. 2011.

[4] Ahmad, A. O., Maddock, C., Scanlon, T., and Brown, R., "Prediction of the aerodynamic performance of re-usable single stage to orbit vehicles," *Space Access 2011*, 2011.

[5] Anderson, J., *Hypersonic and High-Temperature Gas Dynamics (Second Edition)*, AIAA, 2006.

[6] Carandente, V., Savino, R., Iacovazzo, M., and Boffa, C., "Aerothermal Analysis of a Sample-Return Reentry Capsule," *Fluid Dynamics & Materials Processing*, Vol. 9, No. 4, 2013, pp. 461–484.

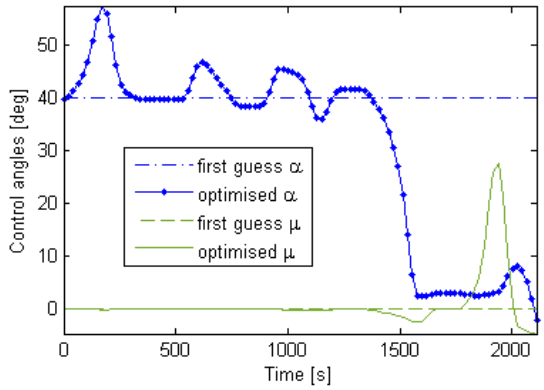


(a) With no thermal constraints

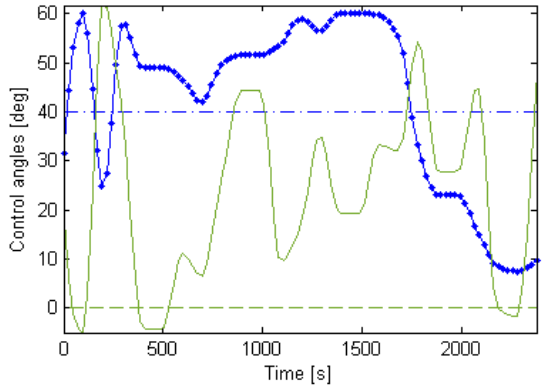


(b) With thermal constraints

Fig. 14: Time history of the angle of attack $\alpha$ and bank angle $\beta$ during the re-entry and glide phases of the descent trajectory.

[7] *AIAA Guide to Reference and Standard Atmosphere Models (G-003C-2010e)*, American Institute of Aeronautics and Astronautics, 2010.

[8] Vinh, N., *Optimal Trajectories in Atmospheric Flight*, Elsevier, New York, 1981.

[9] Shen, H. and Tsiotras, P., "Using Battin's method to obtain multiple-revolution Lambert's solutions," *Advances in the Astronautical Sciences*, Vol. 116, 2004, pp. 1–18.

[10] Battin, R. H., *An introduction to the mathematics and methods of astrodynamics*, AiAA, 1999.

[11] Kaplan, G. H., "The IAU Resolutions on Astronomical Reference Systems, Time Scales, and Earth Rotation Models: Explanation and Implementation," Circular 179, US Naval Observatory, 2005.

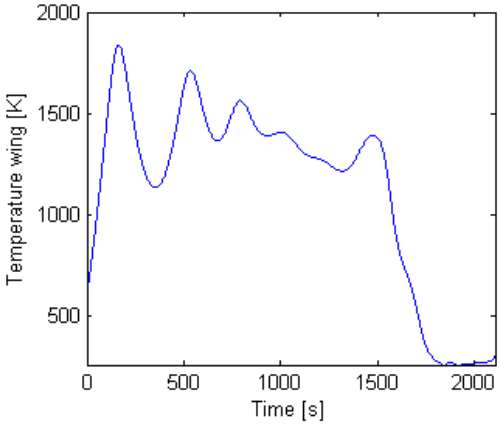


(a) Temperature on the leading edge of the wing

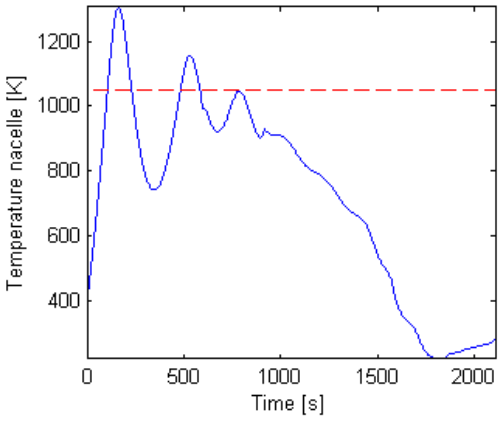


(b) Temperature on the nacelle

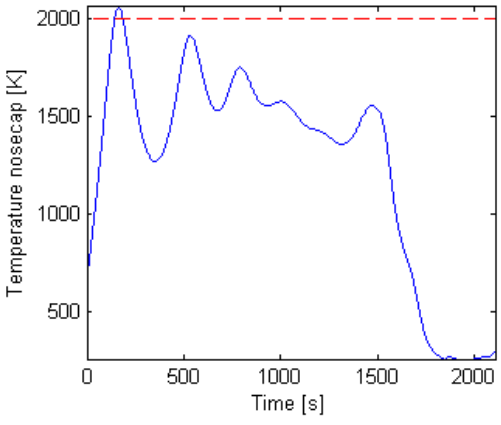


(c) Temperature on the nose

Fig. 15: Temperatures on the vehicle surface during the descent for the case with no thermal constraints

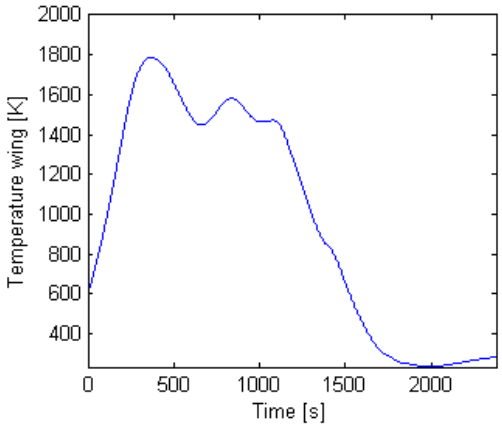


(a) Temperature on the leading edge of the wing

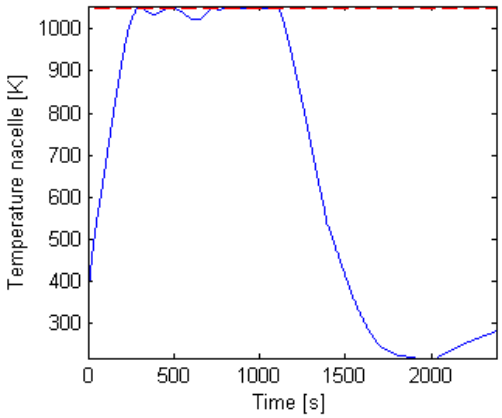


(b) Temperature on the nacelle

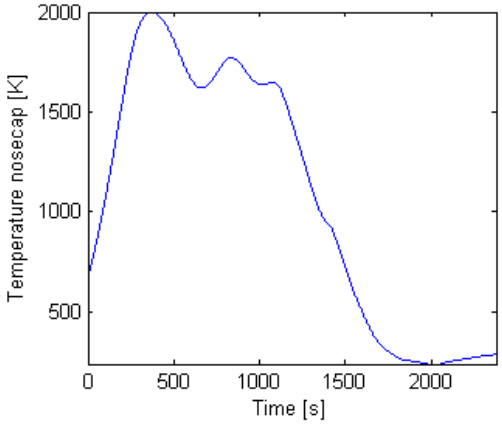


(c) Temperature on the nose

Fig. 16: Temperatures on the vehicle surface during the descent for the case with thermal constraints